**Astronomy
&
Astrophysics**

A detailed observation of a LMC supernova remnant DEM L241 with *XMM-Newton*[⋆]

A. Bamba[1], M. Ueno[2], H. Nakajima[3], K. Mori[4], and K. Koyama[3]

1. RIKEN (The Institute of Physical and Chemical Research) 2-1, Hirosawa, Wako, Saitama 351-0198, Japan
   e-mail: bamba@crab.riken.jp
2. Department of physics, Faculty of Science, Tokyo Institute of Technology 2-12-1, Oo-okayama, Meguro-ku, Tokyo 152-8551, Japan
   e-mail: masaru@hp.phys.titech.ac.jp
3. Department of Physics, Graduate School of Science, Kyoto University, Sakyo-ku, Kyoto 606-8502, Japan
   e-mail: [nakajima;koyama]@cr.scphys.kyoto-u.ac.jp
4. Department of Applied Physics, Faculty of Engineering University of Miyazaki, 1-1 Gakuen Kibana-dai Nishi Miyazaki, 889-2192, Japan
   e-mail: mori@astro.miyazaki-u.ac.jp

ABSTRACT

We report on an *XMM-Newton* observation of the supernova remnant (SNR) DEM L241 in the Large Magellanic Cloud. In the soft band image, the emission shows an elongated structure, like a killifish, with a central compact source. The compact source is point-like, and named XMMU J053559.3−673509. The source spectrum is reproduced well by a power-law model with a photon index of $\Gamma = 1.57$ (1.51–1.62); and the intrinsic luminosity is 2.2×10^{35} erg s^{-1} in the 0.5–10.0 keV band, with an assumed distance of 50 kpc. The source has neither significant coherent pulsations in 2.0×10^{-3}–8.0 Hz nor time variabilities. Its luminosity and spectrum suggest that the source might be a pulsar wind nebula (PWN) in DEM L241. The spectral feature classifies this source as rather bright and hard PWN, which is similar to those in Kes 75 and B0540−693. The elongated diffuse structure can be divided into a "Head" and "Tail", and both have soft and line-rich spectra. Their spectra are reproduced well by a plane-parallel shock plasma (*vpshock*) model with a temperature of 0.3–0.4 keV, over-abundance in O and Ne, and a relative under-abundance in Fe. Such an abundance pattern and the morphology imply both that the emission is from the ejecta of the SNR and that the progenitor of DEM L241 is a very massive star, more than 20 $M_\odot$. This result is also supported by the existence of the central point source and an OB star association, LH 88. The total thermal energy and plasma mass are $\sim 4 \times 10^{50}$ erg and ~ 200 $M_\odot$, respectively.

Key words. ISM: supernova remnants – X-rays: individual: DEM L241 – X-rays: individual: XMMU J053559.3–673509

1. Introduction

Supernovae (SNe) and supernova remnants (SNRs) shape and enrich the chemical and dynamical structure of the interstellar medium and clouds. X-ray studies give us plenty of information about hot plasma in SNRs with emission lines from highly ionized ions. Moreover, SNRs are believed to be cosmic ray accelerators around their pulsar and pulsar wind nebula (PWN) and/or shock fronts. The Magellanic Clouds (MCs) are the best galaxies for systematic study of SNRs, thanks to the known distance (50 kpc; Feast 1999) and the small absorption column. Another subject of interest is supernova explosions in starburst galaxies. The SNe of massive stars scatter light elements into such galaxies, and make an abundance pattern different from those in normal galaxies (e.g., Umeda et al. 2002). The Large Magellanic Cloud (LMC) is the nearest starburst

galaxy (Vallenari et al. 1996), so we can examine the influence of discrete massive SNe on the galaxy. Now, more than 30 LMC SNRs are cataloged (Williams et al. 1999) and the number may still increase (e.g., Chu et al. 2004). However, we only have a few samples for which the type and age are known.

The pulsars and their nebulae offer clear evidence of a core-collapsed origin and are good indicators of their age. Now, only four LMC SNRs are reported to have a pulsar and/or PWN; B0540−693 (Manchester et al. 1993), N157B (Wang et al. 2001), B0532−710 (Klinger et al. 2002; Williams et al. 2005), and B0453−685 (Gaensler et al. 2003). This is mainly because of a lack of spatial resolution in previous radio and X-ray observations. Thus, searching for new SNR containing pulsars and PWNe in the LMC is critical for carrying out a systematic study of the contributions from SNRs to interstellar medium in th LMC.

DEM L241 (0536−67.6) was identified as an SNR by Mathewson et al. (1985). They found that DEM L241 shows the typical looped filamentary structure of an SNR with a size

---

of ~2′ in the optical image. The [S II] to Hα ratio is 0.6 (Mathewson et al. 1985), which is typical of the ratio for SNRs. Radio emission in 843 MHz was also reported by Mathewson et al. (1985), which shows a shell-like structure similar in size to the optical shell. *Einstein* detected relatively bright X-rays (2.7×10^{35} erg s^{-1} in the 0.15–4.5 keV band, Mathewson et al. 1985). It appears to be a blow-out of the dense H II region, N 59B, around the OB star association LH 88 (Chu & Kennicutt 1988). A study of the echelle spectrum by Chu (1997) shows a relatively small expansion velocity and a large intrinsic velocity width, implying that the SNR may be expanding within the stellar-wind blown cavity, which suggests that the progenitor of DEM L241 is likely to be a massive star. Nishiuchi (2001) observed this SNR with *ASCA*, and found that the spectrum of the remnant requires not only thermal emission but also a power-law component with Γ ~ 1.6. This result indicates that DEM L241 has a pulsar and/or a PWN, or synchrotron X-ray emitting shells like SN 1006 (Koyama et al. 1995; Bamba et al. 2003). However, the lack of spatial resolution for *ASCA* prevented us from making a definite conclusion about the origin of the hard X-ray emission.

In this paper, we report the detailed X-ray analysis of DEM L241 for the first time using *XMM-Newton*, with the help of *ASCA* data. Section 2 summarizes the details of *XMM-Newton* and *ASCA* observations of DEM L241. The results of the analysis are found in Sect. 3, while Sect. 4 is devoted to discussion of the origin of the remnant. We assume the distance to the LMC to be 50 kpc (Feast 1999) in this paper.

2. Observations and data reduction

The *XMM-Newton* (Jansen et al. 2001) EPIC cameras (Strüder et al. 2001; Turner et al. 2001) observed DEM L241 on December 29, 2004 (observation ID = 0205380101). The on-axis point spread function (PSF) is 5″ for MOS CCDs and 6″ for pn, in full-width half maximum. The medium filter was used for all three EPIC cameras to block ultraviolet photons (Stephan et al. 1996; Villa et al. 1998). In this observation, both EPIC MOS and pn cameras were operated in the full frame mode providing a time resolution of 2.6 s and 73.4 ms, respectively. The data reductions and analysis were made using Science Analysis System (SAS) software version 6.1.0. We filtered out background flares for rates in >10 keV band higher than 0.35 (1.0) counts s^{-1} for the MOS (pn) cameras, resulting in 45 (43) ks of good time intervals. In the following analysis, we use the grade pattern 0–12 events for MOS data and 0–4 events for pn data, according to the SAS guide.

For the timing analysis, we used *ASCA* (Tanaka et al. 1994) GIS (Gas Imaging Spectrometer, Ohashi et al. 1996) screened archive data of DEM L241, because GIS has better time resolution than pn. The observation was carried out on October 12–14, 1999. Two GISs (GIS2 and GIS3) were operated in the nominal pulse height mode. Only high bit data was used, which provides the best time resolution of 62.5 ms. The total exposure time is 42 ks for both GISs. To increase the statistics, the data of the two detectors, GIS2 and GIS3, were combined in the following study.
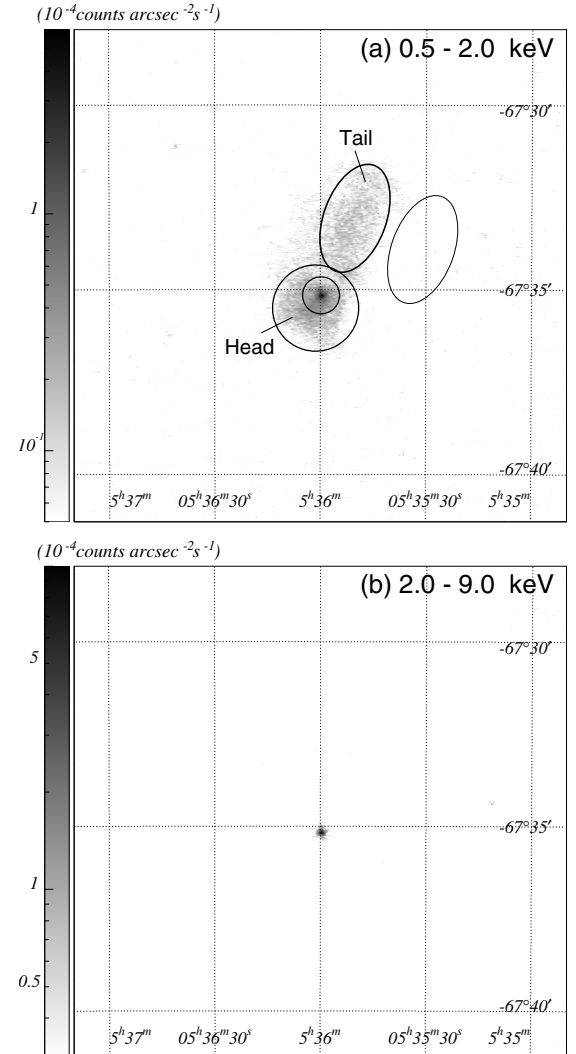

Fig. 1. MOS 1+2 images in the **a)** 0.5–2.0 keV and **b)** 2.0–9.0 keV bands with J2000 coordinates. The scales are logarithmic with units of ×10^{-4} counts s^{-1} arcsec^{-2} cm^{-2}, as shown in the left bar for each image. Each picture is binned with 20 pixels each and smoothed with 1″ scale. The source and background regions used for the spectral analyses are shown by the solid thick and thin lines in the panel **a)**.

3. Results

3.1. Image analysis

Figure 1 shows the *XMM-Newton* MOS 1+2 images of DEM L241 in the (a) 0.5–2.0 keV and (b) 2.0–9.0 keV bands. The correction of the exposure time was performed, whereas the subtraction of background photons was not carried out. In the soft band image, we can see a diffuse structure elongated from southeast to northwest with the size of ~1′.5 × 3′, corresponding to 22 pc × 44 pc at 50 kpc. The shape is like a killifish, with a double-peaked feature on its "Head" and "Tail" (see Fig. 1). In addition to the body of the fish, there is a compact source like an "eye" of the fish. On the other hand, only the eye can be seen in the hard band image.

We determined the position of the point-like source with the MOS 1+2 image, using the `edetect` command in SAS,
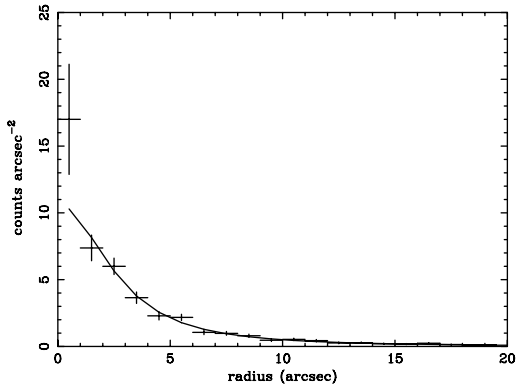
Fig. 2. MOS 1+2 radial profile of Source 1 in the 2.0–9.0 keV band. The solid curve and crosses represent the best-fit King profile model and data, respectively.
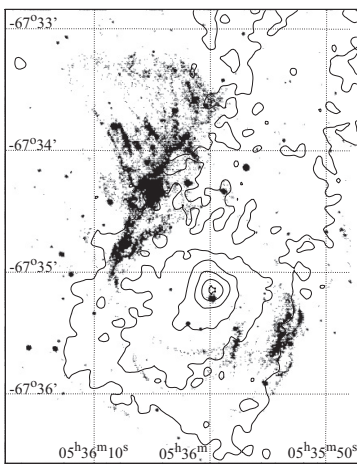

Fig. 3. The [S II] gray-scale map (Mathewson et al. 1985) overlaid on the MOS 1+2 0.5–9.0 keV contour map with J2000 coordinates. The contour is in the logarithmic scale.

Fig. 4. Spectra of the Source 1 **a)**, Head **b)**, and Tail **c)** regions. Although we fitted the spectra of MOS 1+2 and pn CCDs simultaneously, only the MOS 1 data and results are shown for brevity. The best-fit models are shown with solid (*vpshock*) and dotted (power-law) lines. Lower panels in figures represent data residuals from the best-fit models.

to be ($05^h35^m59.93$, $-67^d35^m09.72$), then named the source as XMMU J053559.3−673509. Although counterparts were searched for with the SIMBAD data base, we found no candidate in any wavelength. Hereafter, we refer to this as Source 1. The radial profile of Source 1 was made with the 2.0–9.0 keV MOS 1+2 data as shown in Fig. 2. The source is as compact as the PSF of *XMM-Newton*. The fitting of the profile with a single King profile model was accepted statistically with reduced χ^2 of 18.0/17. The best-fit core radius is $3.''1$ ($2.''4$–$3.''9$) (hereafter, the parentheses indicate single parameter 90% confidence regions), which is the same as the PSF of MOS CCDs. Therefore, we concluded that Source 1 is not significantly extended. The upper-limit of the source size is 1.0 pc.

Figure 3 shows the [S II] gray-scale image (Mathewson et al. 1985), overlaid on the MOS 1+2 0.5–9.0 keV contour map. The [S II] emission, which traces the shock front, surrounds the Head region with two strong and weak rims on northeastern and southwestern sides. The 843 MHz map by Mathewson et al. (1985) basically agrees with the [S II] map. The northern part of the Head is also bright in the light of [O III] (Mathewson et al. 1985). There is no enhancement around the Tail region in both [S II] and radio maps, although the field
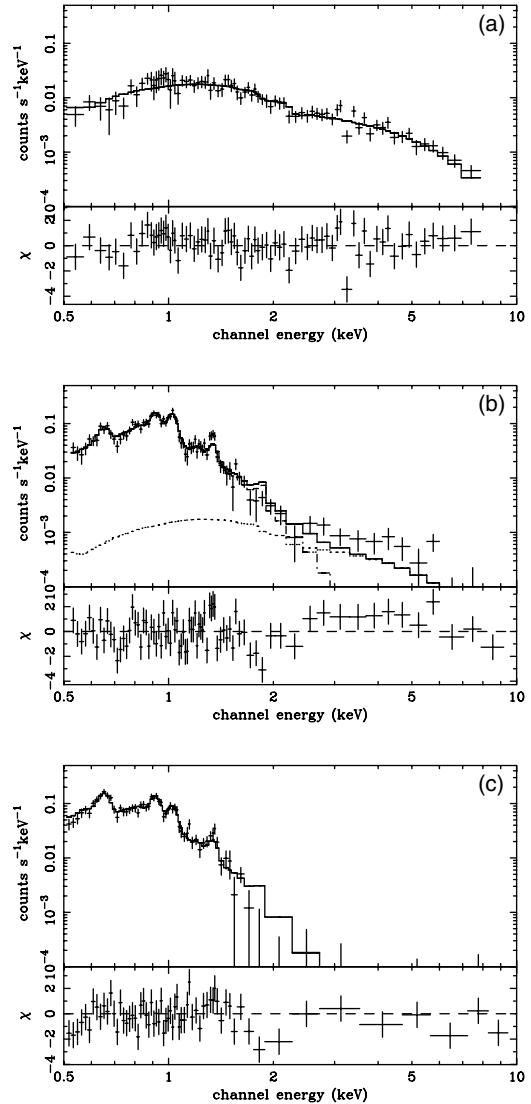
of view of the [S II] map is too small to cover the whole Tail region.

3.2. Spectral analysis

3.2.1. Source 1

The spectrum of Source 1 was accumulated from a $15''$ radius circle around the source for each detector. The background annular region was selected with $20''$ inner radius and $30''$ outer radius. Figure 4a shows the background subtracted spectrum of Source 1, which is very hard and has no line-like structure. We fitted the spectra of the three detectors simultaneously with a power-law function plus absorptions. The galactic and LMC absorptions (N_H^{gal} and N_H^{LMC}, respectively) were calculated separately. We fixed N_H^{gal} to be

Table 1. Best-fit parameters for Source 1[a].

Parameters	
Γ	1.57 (1.51–1.62)
$N_{\rm H}^{\rm LMC}$ [10^{21} cm^{-2}][c]	3.3 (2.7–4.0)
Flux [10^{-13} erg cm^{-2} s^{-1}][c]	6.4 (6.0–6.8)

[a] Parentheses indicate single parameter 90% confidence regions.
[b] Calculated using the cross sections by Morrison & McCammon (1983) with the average LMC abundances (Russell & Dopita 1992).
[c] In 0.5–10.0 keV band.

5.56×10^{20} cm^{-2}, which is estimated by Dickey & Lockman (1990), whereas $N_{\rm H}^{\rm LMC}$ was treated as a free parameter. Each absorption column was subsequently calculated using the cross sections by Morrison & McCammon (1983), with the solar abundances (Anders & Grevesse 1989) for $N_{\rm H}^{\rm gal}$, and the cross sections by Balucinska-Church & McCammon (1992), with the average LMC abundances (0.3; Russell & Dopita 1992; Hughes et al. 1998) for $N_{\rm H}^{\rm LMC}$. The fitting was acceptable with the reduced χ^2 of 365.1/376. The best-fit model and parameters are shown in Fig. 4a and Table 1.

3.2.2. Diffuse emission

The diffuse emission in DEM L241 shows an elongated structure with a "Head" and "Tail". We divided the emission into the Head and Tail regions as shown in Fig. 1a. The source region for the spectral analysis of the Head was made from a 70″ radius circle region excluding a 30″ radius circle around Source 1. On the other hand, the region for the Tail was taken as an elliptical shape with 50″ × 90″ radii. The background photons were accumulated from a source-free region near the SNR. These regions are shown in Fig. 1a with thick (for the sources) and thin (for the background) lines.

Figures 4b and c show the background-subtracted spectra of the Head and Tail regions. The spectra are basically soft and have a line-like structure, implying that there is at least a thermal emission component. The center energies of these lines agree with He-like O, He-like Ne, and He-like Mg. The Head spectrum has an additional hard tail, which is probably contamination from the bright Source 1, since the fractional encircled energy within 30″ is only ~90%.

We used the spectra of the three CCDs simultaneously and fitted them with a plane-parallel shock plasma (*vpshock*) model (Borkowski et al. 2001), packaged in `xspec` 11.3.1., with the galactic and LMC absorptions. The absorption calculation was done in the same way as the Source 1 case (see Sect. 3.2.1). The abundances of the plasma were fixed to 0.3 (Russell & Dopita 1992; Hughes et al. 1998). For the spectrum of the Head region, we added an additional power-law component that represents contamination from Source 1. The value of Γ was fixed as 1.57, the best-fit value for Source 1 (Table 1). The fittings were rejected with the χ^2/d.o.f. of 871.8/381 (Head) and 607.1/300 (Tail), with sinusoidal residuals around O and Ne lines. Therefore, we allowed O, Ne, and Fe abundances to vary freely following the previous result by Hughes et al. (1998). The fits were greatly improved and accepted

Table 2. Best-fit parameters for the diffuse emission[a].

Parameters	Head	Tail
vpshock		
$kT_{\rm e}$ [keV]	0.39 (0.38–0.40)	0.35 (0.34–0.39)
$n_{\rm e}t_{\rm p}$ [10^{12} cm^{-3} s]	(>14.6)	9.0 (>2.0)
[O/H][b]	0.36 (0.30–0.47)	0.47 (0.36–0.64)
[Ne/H][b]	0.82 (0.74–0.96)	0.79 (0.63–1.0)
[Fe/H][b]	0.09 (0.07–0.11)	0.11 (0.09–0.15)
E.M. [10^{58} cm^{-3}][c]	4.4 (3.8–4.8)	2.8 (2.1–3.5)
$N_{\rm H}^{\rm LMC}$ [10^{21} cm^{-2}][d]	5.6 (4.7–6.4)	1.8 (1.0–3.1)
Flux [10^{-13} erg cm^{-2} s^{-1}][e]	3.2	3.6
Power-law[f]		
Flux [10^{-14} erg cm^{-2} s^{-1}][e]	4.6 (3.6–5.6)	–

[a] Parentheses indicate single parameter 90% confidence regions.
[b] Abundance ratio relative to the solar value (Anders & Grevesse 1989). [c] $E.M. = n_{\rm e}^2 V$, where $n_{\rm e}$ and V are the electron density and the volume, respectively. [d] Calculated using the photometric absorption cross-sections by Balucinska-Church & McCammon (1992) with the LMC abundances (Russell & Dopita 1992). [e] In the 0.5–10.0 keV band. [f] Γ is fixed to the best-fit value for Source 1 (1.57).

statistically for both regions with reduced χ^2 of 505.3/377 (Head) and 333.9/296 (Tail). The best-fit models and parameters are shown in Figs. 4b and 4c and Table 2, respectively. We tried but gave up leaving the abundance of Si free, because there is a strong background emission line (Katayama et al. 2004).

The flux of the power-law component in the Head region is 6.4 ± 1.3%, which is consistent with the expected contamination of Source 1. Thus, we concluded that this hard excess is only due to the contamination of Source 1, and do not mention this component hereafter.

3.3. Timing analysis

Coherent pulsations were searched for in Source 1. We extracted photons from the 2.0–8.0 keV band (Source 1 is bright in this band as seen in Fig. 4a) and from a 15″ radius circle around Source 1. The correction of the photon arrival times was made to those at the barycenter. A fast Fourier transform (FFT) algorithm was applied to the pulsation search. We used all three instruments for the pulsation search from 2×10^{-3} Hz to 0.19 Hz and only the pn CCD, which has better time resolution than the MOS CCDs, for the 0.19–6.8 Hz search. The resulting power density spectra (Figs. 5a,b) show no significant peak from 2×10^{-3} Hz to 6.8 Hz. Although we also analyzed timing data accumulated from a 5″ radius circle and/or photons in other wider and narrower bands, the results did not change significantly.

We also conducted the timing analysis with *ASCA* GIS data, which has better time resolution than MOS and pn. The source photons were accumulated from a 3′ radius circle around Source 1, within the 2.0–8.0 keV band. After correcting the photon arrival times to those at the barycenter, we applied an FFT algorithm to search the coherent pulsation. No significant pulsation was found up to 8.0 Hz again, as can be seen in Fig. 5c.
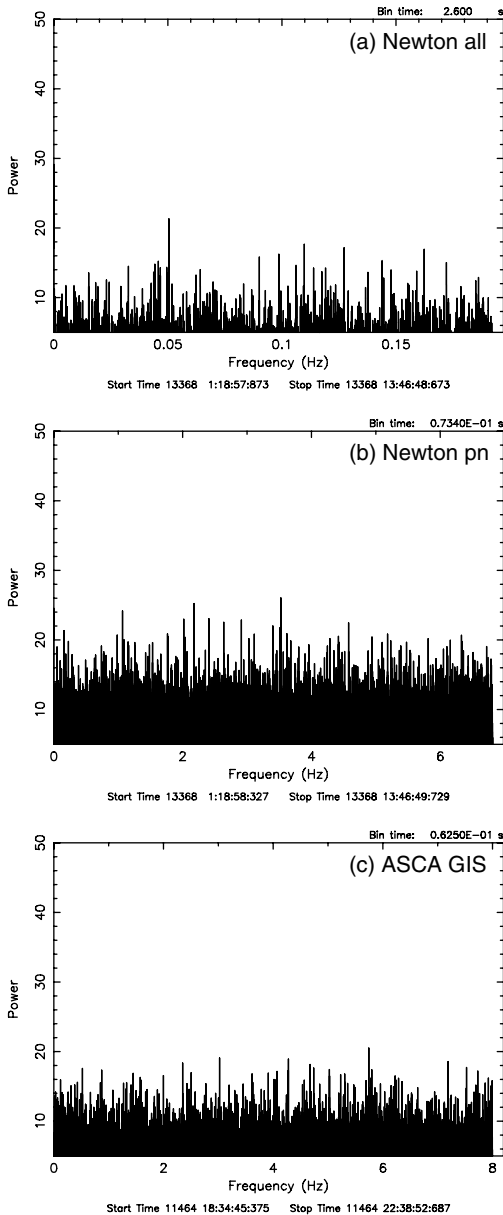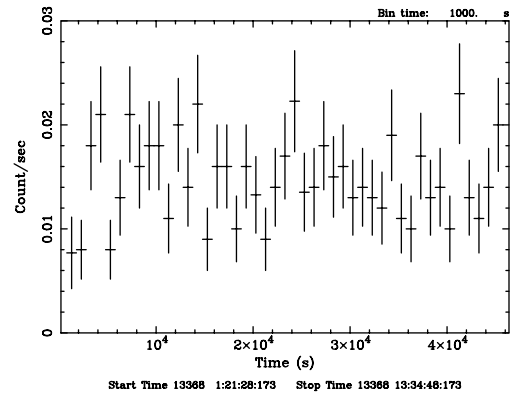
Fig. 6. X-ray light curves of Source 1 with MOS1+2 and pn CCDs in the 2.0–8.0 keV band (bin time = 1 ks).

excess might be due to the H I excess reported in the H I map by Stavely-Smith et al. (1998). However, we can conclude nothing due to the lack of high sensitivity information around the SNR. More H I observations with better spatial resolution are required to discuss this issue quantitatively.

4.2. Source 1

The central position of Source 1, the hard spectrum, and persistent luminosity indicate that Source 1 might be a pulsar and/or a PWN of DEM L241. The lack of detection of coherent pulsation is not surprising, since the periods of ordinary rotation-powered pulsars detected with X-rays are $\lesssim 0.1$ s. The hard spectrum also resembles the emission from background active galactic nuclei (AGNs), although the source shows no time variability. We estimate the probability of chance coincidence that a background AGN is accidentally in the SNR region. With the $\log N$–$\log S$ relation of AGNs derived by Hasinger et al. (1998), we found that the expected number of AGNs is only 1.1×10^{-3} in the $1.5' \times 3'$ region. Therefore, we concluded that Source 1 is an LMC member. The similarity of the absorption column for Source 1 to that of the Head region also supports that. In the case that Source 1 is a pulsar and/or a PWN, this adds a new member to the sample of LMC PWNe (Gaensler et al. 2003). The hard X-ray flux detected by *ASCA* (Nishiuchi 2001) is consistent with that of Source 1. Thus we consider that the hard X-rays are not from energetic electrons accelerated on the shell but the central point source. The distance from Source 1 to the center of LH 88 is about $14''$, and the diaphragm diameter of LH 88 is $100''$ (Bica et al. 1996), so the progenitor might be a member of the cluster.

The intrinsic luminosity of Source 1 is 2.2×10^{35} erg s^{-1} in the 0.5–10.0 keV band under the assumption that the distance to Source 1 is 50 kpc, and the photon index is 1.57 (1.51–1.62). The luminosity and hardness ranges of pulsars are wide, $\log L_{\mathrm{x}} \sim 31$–36, $\Gamma \sim 0.6$–2.0, respectively (e.g., Gotthelf & Olbert 2001; Gaensler et al. 2003). Recently, "compact central sources" have been discovered in several SNRs (Cas A, Chakrabarty et al. 2001; Vela Jr., Kargaltsev et al. 2002; Kes 79, Seward et al. 2003), which have rather small luminosities ($\log L_{\mathrm{x}} \sim 32$–34) and soft spectra ($\Gamma = 3$–4). In the case that

Fig. 5. The power density spectra with the MOS1+2 and pn **a)**, pn **b)**, and *ASCA* GIS2+3 **c)**. Data points are plotted only when its power is higher than 5.

Figure 6 shows the light curve of Source 1 in the 2.0–8.0 keV band, which is the combined result of the three *XMM-Newton* detectors. We applied the Kolmogorov-Smirnov test for this light curve and found that Source 1 has no significant time variability during the observation with the probability of constancy of 0.72.

4. Discussion

4.1. The absorption

The best-fit $N_{\mathrm{H}}^{\mathrm{LMC}}$ in our analysis is almost consistent with or slightly larger than the LMC absorption column estimated from the 21 cm line survey (8.4×10^{20} cm^{-2}; Rohlfs et al. 1984), implying that this source is in the LMC. The small

Source 1 is a pulsar or a compact central source, Source 1 is one of the brightest samples, as bright as the Crab pulsar (Pravdo et al. 1997). Such bright pulsars certainly have PWNe, which are about 10 times brighter than the pulsars themselves and also have hard spectra (log L_x = 33–37 and Γ = 1.3–2.3; Gotthelf & Olbert 2001). Thus, we conclude that the emission is from a PWN of DEM L241. Its photon index is rather small for ordinary PWNe and is similar to those of the PWN in Kes 75 (Helfand et al. 2003) and B0540−693 (Hirayama et al. 2002). Helfand et al. (2003) notes that these pulsar systems change their energy into X-ray radiation very efficiently. It may be a new sample of such energetic PWNe. Source 1 is moderately bright for PWNe, which might imply that the system is middle-aged. Pulsars in such PWNe have periods of less than a few hundred ms and luminosities of about 10% of their nebulae. Therefore it is natural that we could not detect the coherent pulsation even in the case that Source 1 has a pulsar.

In order to confirm the origin of Source 1, it is essential to resolve the pulsar spatially and to detect coherent pulsations. Therefore, further observations are encouraged with better time and spatial resolution, and of course with excellent statistics, in the X-ray and radio bands.

4.3. Diffuse emission

The temperature and abundance pattern of the hot plasma in the Head and Tail regions are roughly the same as each other statistically, (Table 2), implying that these plasmas have the same origin. The overabundant O and Ne compared to the average LMC indicate that the plasma emission is from the ejecta of the explosion and that relative to Fe implies that the progenitor of DEM L241 may be a core-collapsed SN (Tsujimoto et al. 1995). The Fe abundance is slightly smaller than the avarage value in the LMC (0.22 Hughes et al. 1998), which might be the local fluctuation of metal. The less abundant O relative to Ne might imply that the progenitor is very massive, $\gtrsim 20\ M_\odot$ (Umeda et al. 2002). Umeda et al. (2002) also insists that fast convective mixing in the progenitor star (Spruit 1992) creates more Ne and less O. Therefore, we concluded that the progenitor of DEM L241 was a very massive star. This conclusion is also supported by the presence of the energetic pulsar candidate and the OB star association, LH 88 (Chu & Kennicutt 1988). The abundance pattern of DEM L241 resembles in the one in a starburst galaxy M 82 (Tsuru et al. 1997). This fact might imply that DEM 241 have been produced in a period of starburst activity by the OB star association. Umeda et al. (2000) and Nakamura et al. (2001) have shown that a large Si/O ratio may be signature of energetic SN explosion ($\gtrsim 10^{51}$ erg). Thus, we need to determine Si abundance with low background observations.

The thermal emission in the Head region has a center-filled morphology even considering the contribution from Source 1. Note that the radius of the extent of the thermal emission is ~70″, while that of Source 1 corresponds to the *XMM-Newton* PSF, ~5″. The structure, the radio shell (Mathewson et al. 1985), and the large size of the SNR (see Sect. 3.1), classify the SNR as mixed-morphology (MM) SNRs

Table 3. Physical parameters of the plasma in Head and Tail[a].

Parameters	Head	Tail
n_e [cm^{-3}]	0.28 (0.26–0.29)	0.27 (0.23–0.30)
t_p [10^6 yr]	(>1.8)	1.1 (>0.2)
E [10^{50} erg][b]	2.9 (2.2–3.7)	0.6 (0.5–0.7)
M [$M_\odot$]	132 (122–137)	89 (76–99)

[a] Parentheses indicate single parameter 90% confidence regions.
[b] Thermal energy E is estimated to be $3n_e VkT$.

(Rho & Petre 1998). However, the over-abundant light elements suggest that the emission is not from interstellar medium but from ejecta, as already mentioned, which is not common for ordinary MM SNRs. Then, we concluded that this SNR is an ejecta-dominant SNR without X-ray emitting shells. The absence of a limb-brightened X-ray shell is expected, since this SNR is in a hot and tenuous bubble (Chu 1997), and it is hard to form the strong shock. The elongated shape of the Tail region, together with the lack of enhancement of [S II] and radio continuum emission around the Tail, might indicate that the plasma was ejected an-isotropically into a low-density region. It is natural to consider that the plasma in the Tail region is a blownout on the basis of the [S II] morphology. Chu (1997) suggests that the SNR could be interacting with the inner walls of a bubble to produce the SNR signature. In such a case, the interacting region is heated and emits thermal X-rays, and the emission certainly traces the shock region, like the [S II] emission. If the thermal emission is, on the other hand, center-filled, then we conclude that the thermal X-rays are not from the interacting region but from the ejecta.

In order to estimate the physical parameters of the plasma, we assumed that (i) the plasma in the Head region is distributed in a sphere with the radius of 70″, excluding a spherical region with the radius of 30″ around Source 1 (total volume $V_{\text{Head}} = 5.6 \times 10^{59}$ cm^3), and that (ii) the Tail region has an ellipsoid distribution with the radii of 50″ × 50″ × 90″ ($V_{\text{Tail}} = 4.0 \times 10^{59}$ cm^3), and then calculated the mean electron density (n_e), the age of the plasma (t_p), the thermal energy ($E \simeq 3n_e VkT$), and the total mass of the plasma ($M = n_e m_p V$, where m_p is the proton mass). The results are summarized in Table 3. The t_p indicates that the SNR is rather aged, which is consistent with the large size of the SNR.

5. Summary

We have conducted a detailed analysis of DEM L241 with *XMM-Newton* for the first time. A summary of our results follows:

1. The X-ray emission shows an elongated morphology with a Head and Tail like a killifish. Its size is about 22 pc × 44 pc at 50 kpc. The [S II] and radio emission surround the Head, whereas there is no enhancement around the Tail.
2. We resolved a central point source, XMMU J053559.3–673509, in DEM L241 for the first time. The source has no counterpart in any wavelength, and neither coherent pulsation nor time variability was found. The spectrum is reproduced well by a power-law model with parameters of

$\Gamma = 1.57$ and an X-ray luminosity of 2.2×10^{35} erg in the 0.5–10.0 keV band, implying that this source is a bright hard PWN in DEM L241.

3. The Head and Tail have soft and line-rich spectra with an over-abundance of O and Ne. The abundance pattern indicates a core-collapse origin from a massive progenitor that is heavier than 20 $M_\odot$ for DEM L241.

References

Anders, E., & Grevesse, N. 1989, Geochim. Cosmochim. Acta, 53, 197

Balucinska-Church, M., & McCammon, D. 1992, ApJ, 400, 699

Bamba, A., Yamazaki, R., Ueno, M., & Koyama, K. 2003, ApJ, 589, 827

Bica, E., Claria, J. J., Dottori, H., Santos, J. F. C., & Piatti, A. E. 1996, ApJS, 102, 57

Borkowski, K. J., Lyerly, W. J., & Reynolds, S. P. 2001, ApJ, 548, 820

Chakrabarty, D., Pivovaroff, M. J., Hernquist, L. E., Heyl, J. S., & Narayan, R. 2001, ApJ, 548, 800

Chu, Y.-H. 1997, AJ, 113, 1815

Chu, Y.-H., & Kennicutt, R. C. 1988, AJ, 96, 1874

Chu, Y.-H., Gruendl, R. A., Chen, C.-H. R., Lazendic, J. S., & Dickel, J. R. 2004, ApJ, 615, 727

Dickey, J. M., & Lockman, F. J. 1990, ARA&A, 28, 215

Feast, M. 1999, PASP, 111, 775

Gaensler, B. M., Hendrick, S. P., Reynolds, S. P., & Borkowski, K. J. 2003, ApJ, 594, L111

Gotthelf, E. V., & Olbert, C. M. 2002, ASP Conf. Ser., 9999 [arXiv:astro-ph/0112017]

Hasinger, G., Burg, R., Giacconi, R., et al. 1998, A&A, 329, 482

Helfand, D. J., Collins, B. F., & Gotthelf, E. V. 2003, ApJ, 582, 783

Hirayama, M., Nagase, F., Endo, T., Kawai, N., & Itoh, M. 2002, MNRAS, 333, 603

Hughes, J. P., Hayashi, I., & Koyama, K. 1998, ApJ, 505, 732

Jansen, F., Lumb, D., Altieri, B., et al. 2001, A&A, 365, L1

Kargaltsev, O., Pavlov, G. G., Sanwal, D., & Garmire, G. P. 2002, ApJ, 580, 1060

Katayama, H., Takahashi, I., Ikebe, Y., Matsushita, K., & Freyberg, M. J. 2004, A&A, 414, 767

Klinger, R. J., Dickel, J. R., Fields, B. D., & Milne, D. K. 2002, AJ, 124, 2135

Koyama, K., Petre, R., Gotthelf, E. V., et al. 1995, Nature, 378, 255

Manchester, R. N., Staveley-Smith, L., & Kesteven, M. J. 1993, ApJ, 411, 756

Mathewson, D. S., Ford, V. L., Tuohy, I. R., et al. 1985, ApJS, 58, 197

Morrison, R., & McCammon, D. 1983, ApJ, 270, 119

Nakamura, T., Umeda, H., Iwamoto, K., et al. 2001, ApJ, 555, 880

Nishiuchi, M. 2001, Ph.D. Thesis, Kyoto University

Ohashi, T., Ebisawa, K., Fukazawa, Y., et al. 1996, PASJ, 48, 157

Pravdo, S. H., Angelini, L., & Harding, A. K. 1997, ApJ, 491, 808

Rho, J., & Petre, R. 1998, ApJ, 503, L167

Rohlfs, K., Kreitschmann, J., Feitzinger, J. V., & Siegman, B. C. 1984, A&A, 137, 343

Russell, S. C., & Dopita, M. A. 1992, ApJ, 384, 508; Nature, 368, 432

Seward, F. D., Slane, P. O., Smith, R. K., & Sun, M. 2003, ApJ, 584, 414

Spruit, H. C. 1992, A&A, 253, 131

Stavely-Smith, L., Kim, S., Putman, M., & Stanimirović, S. 1998, Reviews of Modern Astronomy, 11, 117

Stephan, K., Reppin, C., Hirschinger, M., et al. 1996, Proc. SPIE, 2808, 421

Strüder, L., Briel, U., Dennerl, K., et al. 2001, A&A, 365, L18

Tanaka, Y., Inoue, H., & Holt, S. S. 1994, PASJ, 46, L37

Tsujimoto, T., Nomoto, K., Yoshii, Y., et al. 1995, MNRAS, 277, 945

Tsuru, T. G., Awaki, H., Koyama, K., & Ptak, A. 1997, PASJ, 49, 619

Turner, M. J. L., Abbey, A., Arnaud, M., et al. 2001, A&A, 365, L27

Umeda, H., Nomoto, K., & Nakamura, T. 2000, in The First Stars, ed. A. Weiss, T. Abel, & V. Hill (Berlin: Springer), 150

Umeda, H., Nomoto, K., Tsuru, T. G., & Matsumoto, H. 2002, ApJ, 578, 855

Vallenari, A., Chiosi, C., Bertelli, G., & Ortolani, S. 1996, A&A, 309, 358

Villa, G. E., et al. 1998, IEEE Trans. Nucl. Sci., 45, 921

Wang, Q. D., Gotthelf, E. V., Chu, Y.-H., & Dickel, J. R. 2001, ApJ, 559, 275

Williams, R. M., Chu, Y., Dickel, J. R., et al. 1999, ApJS, 123, 467

Williams, R. M., Chu, Y.-H., Dickel, J. R., et al. 2005, ApJ, 628, 704